Understanding the adsorptive and photoactivity properties of Ag-graphene oxide nanocomposites

R.D. Martínez-Orozco[†], H.C. Rosu[†], Soo-Wohn Lee[‡], V. Rodríguez-González[†1]

[†] IPICyT, Instituto Potosino de Investigacion Cientifica y Tecnologica,
Camino a la Presa San José 2055, Col. Lomas 4a. sección, C.P. 78216 San Luis Potosí, Mexico
[‡] Department of Environmental Engineering, Sun Moon University,
Asan, Republic of Korea

Abstract

Nanocomposites of graphene oxide (GO) and silver nanoparticles (AgNPs) were synthetized using a practical photochemical silver functionalization. Their photocatalytic activities were evaluated with two dyes, Rhodamine B and Indigo Carmine, under visible-light irradiation. The prepared nanocomposites were characterized by HRTEM, FESEM, XRD, Raman, FTIR and UV-vis absorption spectroscopy. These nanocomposites present new defect domains of sp^3 type in combination with several graphitic functional groups that act as nucleation sites for anchoring AgNPs, while the spNanocomposites of graphene oxide (GO) and silver nanoparticles (AgNPs) were synthetized using a practical photochemical silver functionalization. Their photocatalytic activities were evaluated with two dyes, Rhodamine B and Indigo Carmine, under visible-light irradiation. The prepared nanocomposites were characterized by HRTEM, FESEM, XRD, Raman, FTIR and UV-vis absorption spectroscopy. These nanocomposites present new defect domains of sp^3 type in combination with several graphitic functional groups that act as nucleation sites for anchoring AgNPs, while the sp^2-sp^3 edge defects domains of GO generate the photoactivity. Furthermore, their photocatalytic performances are governed by their large adsorption capacity, and strong interaction with dye chromophores. A comprehensive photocatalytic way underlying the importance of adsorption is suggested to explain the low visible-light responsive photoactivity of the AgNPs-GO nanocomposites and the possible binding-site saturation. Then, the usage of H2SO4 allows the production of ionic species and helps to confirm the strong adsorption of both dyes. The ability to synthesize AgNPs-GO nanocomposites with extensive adsorptive capacity is certainly of interest for the efficient removal of hazardous materials.

Highlights

- The AgNPs-GO nanocomposites are easily produced by photo-impregnation of GO.
- Defect domains of sp^3 type of GO act as nucleation sites for anchoring AgNPs.
- The cleavage of IC over the GO surface dominates the rate of degradation.
- The AgNPs-GO nanocomposites present extensive Rhb and IC adsorptive capacity.
- GO synthesis produces edge defects domains and functional groups for dye cleavage.

---

[1]Corresponding author. E-mail: vicente.rdz@ipicyt.edu.mx

1. Introduction

Graphene has been in recent years the source of a huge level of interest throughout the scientific community because of its outstanding electronic, mechanical and not in the last place for its photocatalytic properties [1-3].

In an ideal world, graphene is just a monolayer of pure sp^2-hybridized carbon atoms, thus having a zero optical band gap and a high electrical conductivity in storing and shuttling electrons [4]. So far, several sophisticated physical methods of synthesis have been developed to produce graphene including micromechanical cleavage of highly oriented pyrolytic graphite (HOPG) [5], sublimation of silicon from silicon carbine [6,7], and thermal epitaxial growth [8,9] or plasma enhanced chemical deposition from a carbon feedstock gas [10]. On the other hand, graphene oxide is another promising alternative material for production of graphene-based nanocomposites as it can be synthesized in large quantities from inexpensive chemical oxidations of graphite powders. Graphene-based nanocomposites present electronic, mechanical and photocatalytic properties comparable with graphene but are more stable [4,11]. Graphene oxide is usually obtained by reacting graphite powders with strong oxidants and acids [12,13]. The resulting materials are hydrophilic and can generate stable and homogeneous colloidal suspensions in a variety of solvents due to the negatively charged GO sheets [14,15]. In other words, GO is the solution-dispersible form of graphene, which makes it attractive for low cost and solution-phase processing.

GO is an excellent candidate for getting graphene-based nanocomposites. According to the Lerf-Klinowski model [16], the basal plane of GO is decorated with functional groups such as hydroxyl group (OH) and epoxy group (COC), whereas carboxyl groups (COOH) are mainly found at the edges. Recently, high resolution transmission electron microscopy studies have confirmed this model of sp^2-sp^3 domains [17] and several publications discussed the role of the superficial functional groups based on FTIR analyses [18,19]. Different from graphene, GO consists of a mixture of sp^2 and sp^3 carbon atoms: the sp^2 carbon atoms are hydrophobic and only connected to the adjacent carbon atoms while the sp^3 carbon atoms are hydrophilic and bounded to the adjacent oxygen-containing functional groups [20,21]. The latter may generate the band gap properties in the graphene oxide layer, and this band gap depends on the nature and fraction of sp^2 carbon atoms [22,23]. Thus, the sp^2-sp^3 domains may act as photocatalyst when they are irradiated with light of energy exceeding their band gap energy. In addition, the coexistence of ionic groups and aromatic sp^2 domains allows GO sheets to participate in a wide range of bonding and interactions. Due to their solubility and wide-open nature, the GO sheets can be functionalized on both sides of the basal planes as well as at the edges [22]. Such double-sided functional decoration not only offers a new class of solution-dispersible platform for performing chemistry but also presents the possibility of a 2D nanoscale building block to form new hybrid materials [24-26]. On the other hand, during the reduction of GO, the graphitic domains grow in size to form a percolated network, leading to partial restoration of electrical conductivity [20]. However, the harsh chemical oxidation reaction and the loss of carbon atoms generate carbon vacancies in the basal plane [27]. This is the primary reason why the electronic properties of reduced graphene oxide (rGO) are degraded compared to few layers graphene. Another problem is generated by the van der Waals and stacking interactions among individual graphene sheets which induce the tendency of the as-reduced graphene layers to form irreversible agglomerates and even their restacking to graphite when graphene dispersions are dried [28]. By incorporation of metallic nanoparticles in the graphene layers, the aggregation problem can be minimized, prevented and even turned reversible [29].

In this work, a practical method for the functionalization of graphene oxide by photochemical deposition of silver nanoparticles is reported. This approach allows the reduction of graphene oxide and we believe to be an attractive route due to some important advantages such as controlled reduction of metal ions without using a reducing agent and convenient technique from the point of view of practical applications. Those facts motivate us to consider the practical and effective photochemical synthesis of Ag nanoparticles (AgNPs) by UV-irradiation as an excellent alternative for preventing aggregation of graphene sheets and highly monodisperse functionalization with AgNPs. In order to understand the photocatalytic properties and the ability to adsorb dyes of synthesized AgNPs-GO nanocomposite, the photocatalytic degradation under visible light and adsorption of model dyes Indigo Carmine (IC) and Rhodamine B (RhB) was carried out.

2. Experimental

2.1. Synthesis of graphene oxide

Graphene oxide was prepared from graphite powders (Sigma-Aldrich) by the Hummers method [13]. In a typical reaction, 1 g of graphite, 0.5 g of NaNO$_3$, and 23 mL of H$_2$SO$_4$ were stirred in an ice bath. 3 g of KMnO$_4$ were slowly added drop by drop afterwards. The solution was transferred to a 35 °C water bath and stirred for about 30 min to form a thick green paste. Then, 40 mL of deionized water was added very slowly followed by stirring for 1 h while the temperature was raised to 98 °C. Finally, 100 mL of deionized water was added followed by the slow addition of 12 mL of H2O2 (30%), turning the color of solution from dark brown to yellowish pale brown. The warm solution was then filtered in vacuum using a nylon membrane (0.45 μm) and washed with deionized water until the pH reached the neutral level of ∼6.5. The final product was stored under vacuum for drying.

2.2. Photochemical functionalization of AgNPs-GO nanocomposites

The functionalization of GO by the AgNPs was carried out by the reduction of AgNO$_3$ onto GO suspension in ethanol using UV-C irradiation. Briefly, a solution ($2 \cdot 10^{-3}$ M) of AgNO$_3$ dissolved in ethanol was added slowly to a homogeneous suspension graphene oxide under vigorous stirring. The quantity of silver nitrate used for photo-reduction was calculated to provide 1 and 2 wt% of metallic silver in the AgNPs-GO nanocomposite. The resulting suspension was stirred for 15 min at room temperature and then irradiated with a commercial germicidal lamp (TecnoLite G15T8, 214 nm, 17 W) for 60 min with vigorous stirring. The average intensity of radiation was 14.5 mW/cm^2 on the surface of the solution, as measured with a radiometer (UVP E29276). The obtained dried samples were labeled as Ag1-GO and Ag2-GO with the Ag loading at about 1 and 2 wt%, respectively.

2.3. Characterization of nanocomposites

The morphology and microstructure analyses of as-obtained AgNPs-GO were performed by means of FESEM and HRTEM microscopies, respectively. FESEM images were obtained by means of a Helios NanoLab 600i equipped with Advanced DualBeam for ultra-high resolution imaging. The mean particle size of AgNPs was determined by HAADF-STEM (high-angle annular dark-field scanning transmission electron microscopy), using a TECNAI 20 Super-Twin equipped microscope with a LaB6 emission gun operating at electron energy source of 200 kV. The growth profiles of the AgNPs were studied by high-resolution transmission electron microscopy (HRTEM). The elemental composition of the nanocomposites was determined by energy dispersive X-ray spectroscopy (EDS) with an EDAX spectrometer fitted to the TEM or SEM. The particle size distribution histograms for the AgNPs were obtained from the measurements of 200-300 AgNPs. The average particle diameter (ds) was calculated by using the following formula: $ds = \Sigma n_i d_i / \Sigma n_i$, where n$_i$ is the number of particles of diameter d$_i$. The crystal structures were analyzed by an X-ray diffractometer (Brucker Advance D8) in the reflection mode with Cu K$_\alpha$ radiation. The angular domain was 5-80° (2 theta). The surface structures were identified by a Micro-Raman spectrometer (Renishaw), conducted with a low-power green laser (100 mW) at 5 nm, using only 1 to 10 mW of the laser power. The UV-visible absorption spectra of all GO dispersions were performed by a UV-visible spectrometer (Cary 5000 UV-Vis-NIR). Fourier transform infrared (FTIR) and Raman spectroscopies were used to analyze the functional groups and oxidation process as well as the properties of the layers (Thermo Nicolet 6700).

2.4. Photocatalytic tests

The photocatalytic activities were evaluated by photodegradation of two dyes: Indigo Carmine and Rhodamine B. IC is an acid dye and RhB is a basic dye. The visible light source used in the photocatalytic tests was a 30 W halogen lamp (Yazawa Corporation) positioned 2 cm away from a home-made slurry reactor in which cold water was circulating to control the room temperature. Samples were held in dark for 60 min to reach adsorption equilibrium before starting the photodegradation process with constant magnetic stirring.

Photocatalytic tests were performed with 0.15 g of samples dispersed in 150 mL of 10 ppm for Indigo Carmine (Aldrich, 98%) and Rhodamine B (Aldrich, 99%) and the kinetic parameters of photodegradation were measured during 2-7 h, depending on the sample, dry air was bubbled during photocatalytic experiments (1 mL s^{-1}). At given time intervals, samples were extracted and filtered through a 0.45 μm nylon filter and then monitored with an UV-vis spectrophotometer (5000 UV-Vis-NIR of Agilent Technologies). To know the

RhB and IC adsorption on the AgNPs-GO nanocomposites in dark conditions, the samples were monitored in identical conditions without UV irradiation and adsorption equilibrium time.

3. Results and discussion

3.1. Structural characterization

Fig. 1 shows the X-ray diffraction pattern of graphite, GO and AgNPs-GO nanocomposites. Pristine graphite XRD pattern revealed the sharp characteristic diffraction peak for graphite at 26.54° of 2 theta a stacking structure. For GO, the observed diffraction peaks, (0 0 2) and (0 0 4), were displaced to a value of approximately 14° of 2 theta, as a result of exfoliation of the graphite layers. The diffraction peaks (1 0 0) and (1 0 1) have not been observed, which can be explained because in oxidizing graphite the exfoliation breaks the symmetry of the graphite structure and the contribution to the reflection of these peaks is zero. The interlayer distance of the (0 0 2) peak planes for GO is 7.3 Å (2 theta = 12.08^o), larger than the original graphite, 3.34 Å, confirming expansion and exfoliation of the graphite layers. Increasing the content of Ag in the composite from 1 to 2 wt% results in a shift; therefore, the gradual shift suggests the reduction and stabilization of graphene oxide. No diffraction peaks attributed to silver particles (Ag^0) were identified and therefore it may be assumed that Ag^0 particles are homogenously distributed as nanometer size particles on the GO surface, which are not detectable by XRD. Xiong et al. report similar XRD results by the incorporation of AuNPs in GO [30]. Kim et al. observed that at higher silver content the diffraction peak of GO is no longer observed, indicating the reduction of GO to rGO [31]. In our research by incorporating 5 wt% of AgNPs the diffraction peak at 12.08^o of 2T corresponding to GO diminished in intensity, Fig. S1 in ESI (Electronic Suplementary Information, Appendix A), and the diffraction peaks for silver particles are observed (Ag^0 JCPDS 04-0783), most probably because the AgNPs agglomerate on the surface of GO. Beyond 5 wt% we do not achieve highly monodisperse AgNPs within GO.

3.2. Morphology and composition

FESEM images are shown in Fig. 2. The FESEM image for Ag1-GO shows the AgNPs anchored onto the GO layers in Fig. 2a. The GO layer looks very thin with only the edges partially folded. The AgNPs distribution and size become uniform, while avoiding aggregation of the graphene layers. The AgNPs are anchored homogeneously, no preference for special sites was observed. Ideally, one would expect monolayers; however we observed few graphene layers of micron size. Similar images are obtained for Ag2-GO, the difference in size is not big, Fig. 2b. For Ag1-GO the mean size is 10 nm, while for Ag2-GO is 15 nm, Fig. 2d. In order to confirm that the photochemical silver functionalization allows complete reduction, the nanocomposite Ag2-GO was treated with a reduction treatment using dimethylformamide (DMF), leading to Ag2-GOPR. Fig. 2c shows the FESEM images of the Ag2-GOPR. They look very similar to those of the same sample without additional reduction. No additional reduction was obtained with the organic reduction. It means that the method of photoreduction used for the functionalization is practical, not toxic, and economic without requiring any additional chemical reducer. The FESEM images for bare GO look similar to those of the functionalized one (not shown).

Furthermore, the EDS analysis of the samples confirms the presence of silver, on a percentage level (by weight) according to the synthesis performed, Fig. 2d. As previously mentioned, the silver concentration in the synthesis was calculated as 1 wt%, the average quantization resulting from chemical analysis shows an average value of 1.06 wt%. The small difference may be explained through the small sampling of the chemical analysis. Krishnamoorthy et al. [32] report a similar exfoliated GO with similar morphology which depicts the sheet-like structure. The photocatalytic GO was also synthesized by Hummers method.

Fig. 3 shows HRTEM images for Ag2-GO nanocomposite. In Fig. 3a, selected AgNPs of size of ~10 nm are observed. The analyzed silver particle shows that the Ag^0 lattice fringe varies about 0.25 nm. However, it can be correlated with the lattice constant for silver (1 1 1), 0.2308 nm, according to the JCPDS standard 04-0783. For the GO prepared by the Hummers method, the interplanar distance measured by the profile on the image was of 0.357 nm corresponding to its GO phase [33]. These results agree well with XRD characterization and FESEM images. Compared to other methods, in this work we obtained well defined AgNPs. For example, Liu et al. [34] obtained monodisperse AgNPs on GO for antibacterial activity using Oleylamide-capped Ag, a case in which the stabilization process (purification-freeze dried) takes around 36 h. Also, Tang et al. [35] reports the growth of AgNPs on graphene using PVP and formaldehyde as a reducing agent. AgNPs grow preferentially in the (1 1 1) plane in a face-centered cubic symmetry. The AgNPs shown in that paper are around 20 nm, and in addition the authors report that the fringe spacing of the graphene

sheet is 0.34 nm. In this work, similar values are obtained, 0.357 nm for the sheet of GO [33]. The difference in the values can be attributed to the functional group attached to the GO sheet. We confirm that with the proposed method, one can obtain quasi-spherical AgNPs around 10 nm with face-centered cubic structure in a very thin GO layer.

3.3. Optical properties

Fig. 4 shows UV-vis absorption spectra of dispersions of Ag1-GO, Ag2-GO, and GO in deionized water (25 μg mL^{-1}). GO exhibits one strong absorption band at 236 nm and a shoulder at around 306 nm, corresponding to $\pi \rightarrow \pi^*$ electronic absorption of aromatic CC bond and the $n \rightarrow \pi^*$ transition of the CO bond, respectively [20,22]. After the incorporation of Ag, the $\pi \rightarrow \pi^*$ transition absorption peak redshifted to 261 nm and the $n \rightarrow \pi^*$ transition absorption peak was barely seen. This could be due to the fact that the CO bonds were significantly reduced because they act as nucleation sites and anchoring silver nanoparticles. The red-shift of $\pi \rightarrow \pi^*$ absorption band of AgNPs-GO at 261 nm compared to the band of GO at 236 nm is consistent with the partial retrieval of conjugated network. The decrease of absorbance peak $\pi \rightarrow \pi^*$ suggests electron withdrawing effects of the silver nanoparticles. Any band attributed to silver plasmon resonance cannot be observed, most probably due to the highly monodisperse AgNPs on the GO. We used a low concentration silver content of 1%, because we aimed to obtain AgNPs below 15 nm as we could confirm with XRD, TEM and FESEM characterizations.

3.4. Vibrational properties

The corresponding Raman spectrum is shown in Fig. 5. The characteristic D and G bands at 1355 and 1595 cm^{-1} are observed in all the materials. In the case of the pristine graphite, these bands occur at 1351 and 1582 cm^{-1}. The D band is a characteristic feature for sp^3 domains in carbon layers and the G band provides information on the in-plane vibrations of sp^2 bonds CC [36,37]. Both bands present blue-shifts, notably G bands shift by 10 cm^{-1} indicating reduction stability in the composites. The intensity of the bands is directly related to the density of defects in AgNPs-GO. Higher intensity of bands means lower density of defects [37]. In this work, the photoreduction results in an increase of the intensity of both bands as the content of AgNPs increases, so that the nature of the CC bonds and defects are stabilized with the silver functionalization. In GO and in the AgNPs-GO, the band D is notably increased in contrast to the graphite, indicating the introduction of defects and possibly new CC domains. The density of defects and the new graphitic domains is important for photocatalytic experiments.

The functional groups present in GO and AgNPs-GO composites are characterized by Fourier transform vibrational spectroscopy (FTIR). As shown in Fig. S2 (in ESI), the spectrum of GO displays the broad O–H stretching in the 3700-2400 cm^{-1} region, and the presence of abundant oxygen groups such as carboxyl groups (C–O) at 1723 cm^{-1}, hydroxyl species around 1400 cm^{-1} and 1235 cm^{-1} (OH deformation and C–OH stretching) and epoxy species at 1050 cm^{-1} and 820 cm^{-1} (C-O-C stretching). The band around 1600 cm^{-1} was constantly attributed to the C=C skeletal ring stretch. However, Dimiev et al. [38] confirmed that the band was assigned to water bending modes. The spectrum of AgNPs-GO shows a slight decrement of the oxygen functional group, because the vibration of the epoxy group C-O-C and hydroxyl group O-H are reduced, which is due probably to the anchored AgNPs. This is supported by SEM images which show that the anchoring of the silver nanoparticles is preferentially on the basal planes, where hydroxyl and epoxy groups have localized according to the Lerf-Klinowsky model [16]. This result suggests significantly deoxygenated GO samples because of AgNPs. These bands are almost absent from the spectrum of graphite thus confirming the conversion of graphite to GO. The obtained FTIR spectra confirm the hydrophilic nature of GO, whereas the incorporation of AgNPs onto GO turns some of the domains of the composites into hydrophobic regions.

In general, the AgNPs-GO nanocomposites are successfully prepared by photochemical reduction of AgN0$_3$. The AgNPs-GO is highly monodisperse, with a mean size of 10 nm for Ag1-GO and 15 nm in the case of Ag2-GO. These nanocomposites present new defect domains (sp^3) in combination with several graphitic functional groups.

3.5. Evaluation of photocatalytic activity

Fig. 6 shows the change of concentration (C/C$_0$) of RhB as a function of time under dark conditions and visible-light irradiation, where C$_0$ and C correspond to the initial and measurement concentration of the RhB solution at time t, respectively. All the catalysts followed pseudo-first-order kinetics and the apparent rate constant estimated by plotting ln(C$_0$/C) versus time, Table 1. As shown in Fig. 6, the visible irradiation practically does not produce photolysis confirming that RhB is very stable under visible irradiation [39].

Adsorption measurements of RhB exhibit a significant decrease in the RhB concentration, indicating a strong interaction between RhB and graphene-based composites. Also, no shift of the main absorption band at 554 nm is observed suggesting a complete cleavage of RhB chromophores (Fig. S3, in appendix A). Ag2-GO nanocomposites show higher adsorption, and apparently, the presence of AgNPs slightly increases the adsorption of the RhB dye. In the recent work of Konkena and Vasudevan [40], it is suggested that the stability of the GO dispersions is a consequence of the negative charge of the GO sheets that develops as a result of ionization of different functional groups present, mainly carboxyl groups. Therefore, if taking into account that AgNPs were anchored preferentially on oxygenated functional groups, this is not complete and perhaps some carboxylic groups are available for the electrostatic interaction between the nanocomposite materials and the basic RhB dye molecule.

Under visible light irradiation, the difference in kinetic degradations of RhB for the three samples is slightly different. Again, Ag2-GO displays the highest activity with a half-time less than 2 min. This is attributed to the fact that it is much easier for RhB to be excited and transfer electrons to GO or AgNPs, then generate free radicals and reactive oxidant species, $H_2O + h^+$, to oxidize the RhB* molecule [39,41]. For this it is sufficient to take into account the work functions of RhB (-5.67 eV) and RhB* (-3.08 eV) [39,41]. Thus, a possible mechanism for photodegradation of the RhB can be offered by considering the work functions of the dye and GO (-4.42 eV), as has been proposed by Zhang [30,39,42] in Scheme 1. RhB* in the presence of visible-light can act as sensitizer and inject excited electrons to an electron-acceptor as graphene to become a cationic dye radical (RhB·$^+$), followed by self-degradation or decomposition by reactive oxygen species (ROSs), which occur through the trapping of the excited electrons by the adsorbed oxygen. In this mechanism, there may also be recombination between the injected electron and surface adsorbed RhB·$^+$ (dotted line in Scheme 1). For the AgNPs-GO composites, electrons injected into the GO can be transferred to AgNPs (-4.26 eV) [43]. This leads to a better separation between the electron and RhB·$^+$. This allows the electron in the conduction band of AgNPs to be trapped by dissolved oxygen to form more ROSs which then degrade the dye adsorbed directly onto AgNPs and enhance the degradation of RhB for Ag2-GO. In contrast with the literature that reports the use of lamps of 350 W [30,39,42], we employ a visible light source with only 30 W in our experiments, which makes the degradation much slower which together with the strong adsorptive capacity are the reasons of the activity loss of the GO supports.

In addition, the irradiation could induce the formation of free radicals (OH·) in solution [44], which oxidize more easily the dye, and therefore RhB$^+$ were adsorbed. The remaining superficial carboxyl groups of GO, COOH + RhB$^+$ = COO-RhB, contribute with H$^+$ to the increase of the acidity [45]. This is seen in measuring the final pH (3.38) compared to the initial pH of solution of RhB at 10 ppm (4.42). It is noteworthy that at the end of all tests, the pH of the solutions decreases. On the other hand, AgNPs can act as electron-mediator for charge separation [46], when the excited dye* transfers electrons to GO. Then, the electrons move to the AgNPs and are trapped by O_2 to produce reactive organic species (ROS) [47]. Also RhB* may transfer electrons to AgNPs. The enhanced activity for the dye RhB degradation seems to be due to the synergic effect of adsorption, electron-mediator for charge separation of AgNPs, and the hydroxyl radicals photogenerated when the AgNPs-GO are exposed to lamp irradiation [48].

The degradation of the IC dye as a function of time is shown in Figs. 7 and S4. The adsorption of IC is important, notably GO significantly adsorbs the IC, Fig. 7a. So, there is a competition between adsorption and photoactivity and the cleavage of IC over the GO surface seems to dominate the rate of degradation.

In the photocatalytic evaluation (Fig. 7b), GO degrades the IC more easily than the nanocomposites AgNPs-GO. In the case of GO, the total decomposition of IC is achieved in 7 h, followed by the Ag2-GO with 54% and Ag1-GO with 40%. The incorporation of silver seems first to inhibit the adsorption of IC and logically the degradation is diminished. Graphene oxide seems to show affinity to species like RhB*, and the degradation is enhancing with the incorporation of AgNPs. So, according to the RhB kinetic parameters in Table 1, it is crucial to have first the adsorption over GO or RhB* interaction over AgNPs. Then the low decomposition is achieved and increased with the silver particles in the case of using RhB as a model contaminant.

On the other hand, IC is well adsorbed over GO, the adsorption diminishes by the incorporation of AgNPs, and when the content of AgNPs is 2% the adsorptive capacity seems to recover slightly.

As is observed in Fig. 7, even after 60 min in the dark conditions before starting the photodegradation process, the adsorption equilibrium is not reached. Because the adsorption is still occurring when the irradiation begins, an experiment of degradation without the adsorption equilibrium time was carried out in order to understand this process. Its evolution in the shown adsorption seems to be not possible to be separated due to dominant adsorption rather than degradation.

A possible explanation of the highest percentage of degradation achieved with the GO is that the incorporation of AgNPs into GO stabilizes the GO by reduction and fixing some of the defects. This partially restores the extended sp^2 CC framework. RhB is probably adsorbed on GO by the $N^+(CH_2CH_3)_2$ group of RhB by means of GO $\pi - \pi$ and cation-π interactions [49], then the remaining carboxylic and methyl groups interact with AgNPs to enhance electronic transfer and help decomposition, Scheme 1. Thus, those molecules or the functional groups on GO can be oxidized or reduced depending on the chemical environment, as was evidenced by the work of Chen et al. [50] on the reduction of palladium nanoparticles supported on GO. The initial pH of RhB experiments was 5.5 and for the IC experiments 4.3, and the final pH for both experiments was 3.2 on average.

In order to understand the adsorption interactions between the graphene-based composites with each model dye, the pH-value of the dye solution was adjusted to 3 using a 0.5 M solution of H_2SO_4. Then, we carried out the photocatalytic tests under identical conditions. It was reported that at acid pH the degradation of RhB and IC was increased [51,52]. The effect of the acid environment is to favor the adsorption rather than dye degradation. Graphene oxide is stabilized by hydrogen bonding, by donating hydrogen from H_2SO_4. In this process the carboxylic groups are protonated by adjacent hydroxyl groups [40]. At the same time, the carboxyl groups can be considered as intermediate functional groups in strong dependence on the pH of GO aqueous medium [38]. The charge and dispersibility of GO composites are directly related to the type and concentration of the ionized groups present at different pH according to the GO method of synthesis [40]. Further studies are required in order to understand the role of H_2SO_4 acid environment in the upon-surface rGO/GO system and its functionality.

The results are shown in Fig. 8 and Table 2. At acid conditions, the degradation of both dyes is slightly improved because the pH-value seems to govern the charge of the reactant as well as the surface charge of the GO. In addition, acid conditions diminish the oxidation of AgNPs in aqueous media because the acid acts as a reducing agent, donating hydrogen from sulfuric acid and then the carboxylic groups are stabilized by hydrogen bonding [40], thereby influencing the electrostatic interaction between nanocomposites and the reactants (RhB/RhB*, IC/IC*, its intermediates and by-products). In Fig. S5 it is shown the photolysis and adsorption at dark conditions of RhB and IC for GO and Ag2-GO samples at pH 3. Photolysis looks unstable, mainly for IC, because the RhB and the created IC intermediaries possibly are protonated by hydrogen from sulfuric acid. The adsorptions of both dyes are increased compared with the adsorption at uncontrolled pH. At pH 3 the AgNPs-GO composites are more positively charged. The protonation of the different ionic species present in the sulfuric acid environment may favor mainly adsorption, electron transfer, and decomposition of the dye/dye* and intermediates. Many research groups have reported the use of GO and rGO as adsorbent materials for dye removal [47,53,54]. Secondary radicals formed by side reactions with SO_4^{2-} components in solution will affect the Indigo Carmine of oxidation on AgNPs-GO. Further studies will be carried out to understand the free radical production using IC as a probe [51]. Other authors reported other factors for the loss of activity by the incorporation of reduced metallic NPs, like the fragmentation of graphene oxide as demonstrated recently by Matsumoto et al. [55]. In the schematic representation of our graphene based-nanocomposites, Scheme 1, these materials have an adsorptive capacity to RhB and hazard by-products formed during photocatalytic decomposition. They achieve the total discoloration in about 6 min due to the dye adsorption and degradation. Reasonably large mineralization is not possible because of the by-products generated during the degradation and the large adsorption. The incorporation of ionic species by adding H_2SO_4 before degradation increases the decomposition rate at only 1.0 min^{-1} confirming the hybrid properties of Ag2-GO for basic RhB degradation. However, for the acid Indigo Carmine the adsorptive capacity is not sufficient to favors the photodegradation. It seems that GO and AgNPs act as individual sites. The incorporation of AgNPs seems to inhibit the adsorption of the IC species even with the addition of H2SO4. Adsorption is crucial for degradation and the way in which the RhB and IC adsorb onto GO may help the degradation of RhB. Further theoretical studies will be performed for understanding the optimal way in which each dye can interact with GO an AgNPs and we hope to report the results in a future communication. Total organic carbon (TOC) measurements were carried out in the first and last samples extracted during photocatalytic monitoring, nevertheless the errors vary considerably, but the estimated mineralization of IC and RhB is less that 10%. It means than probably less that 10% of dye was mineralized to CO2 and water. Degradation of dyes only implies the destruction of the chromophore part of the dyes. TOC in adsorption does not show degradation. In Fig. S6 the evolution of RhB adsorption-degradation is shown in three cycles, in identical conditions, as a function of time. The reusing of the catalyst Ag2-GO under UV irradiation seems to slowly saturate the binding-site, although at this conditions it is difficult to separate the photocatalytic process from dominant adsorption. The percentages of degradation by UV-vis

are shown in each experiment, only in the first cycle. The degradation was achieved in about 5 min, in the subsequent cycles, partial decomposition was achieved in 30 min.

The function of the AgNPs-GO composites was improved by using H_2SO_4 in the photocatalytic degradation of Indigo Carmine because of the negatively charged IC. In the case of RhB, a negligible effect is observed due to the enhanced adsorption. Sulfuric acid may help the electron transfer and adjust the adsorption between the GO and the hazard dyes and by-products. Other studies show that SO_4^{2-} ions can be anchored on the surface of TiO_2, developing strong acidity [56]. It is possible that the sulfate ion forms SO and O-S-O bonds in bulk and surface of GO, creating unbalanced charge on sp^2-sp^3 edge domains, vacancies, and defects in the graphene-based composite network. However, further studies are necessary to understand the role of H_2SO_4 acid environment in the context of the rGO/GO surface and its functionality.

4. Conclusion

The AgNPs-GO nanocomposites are easily produced by photo-impregnation of GO in aqueous solution. No further reducing toxic agents were necessary to get very highly monodisperse AgNPs smaller than 15 nm. The visible-light photocatalytic decomposition rates of RhB and IC are low due to the strong adsorption of dyes over AgNPs with GO. The AgNPs-GO composites present an interesting extensive adsorptive capacity in the case of RhB and IC dyes. The function of AgNPs-GO was studied by adjusting the aqueous environment at acid conditions using H2SO4. We find that GO favors the adsorption and decomposition of basic dye species like RhB. This work provides a method of getting in easy way graphene-based nanocomposites for removing hazardous contaminates from wastewater.

References

[1] F. Bonaccorso, Z. Sun, T. Hasan, A.C. Ferrari Graphene photonics and optoelectronics Nat. Photon., 4 (2010), pp. 611-622

[2] M. Liu, X. Yin, X. Zhang Double-layer graphene optical modulator Nano Lett., 12 (2012), pp. 1482-1485

[3] J.O. Hwang, J.S. Park, D.S. Choi, J.Y. Kim, S.H. Lee, K.E. Lee, Y.-H. Kim, M.H. Song, S. Yoo, S.O. Kim Workfunction-tunable, n-doped reduced graphene transparent electrodes for high-performance polymer light-emitting diodes ACS Nano, 6 (2012), pp. 159-167

[4] S. Stankovich, D.A. Dikin, G.H.B. Dommett, K.M. Kohlhaas, E.J. Zimney, E.A. Stach, R.D. Piner, S.T. Nguyen, R.S. Ruoff Graphene based-composite materials Nature, 442 (2006), pp. 282-286

[5] K.S. Novoselov, D. Jiang, F. Schedin, T.J. Booth, V.V. Khotkevich, S.V. Morozov, A.K. Geim Two-dimensional atomic crystals Proc. Natl. Acad. Sci. USA, 102 (2005), pp. 10451-15453

[6] C. Berger, Z. Song, X. Li, X. Wu, N. Brown, C. Naud, D. Mayou, T. Li, J. Hass, A.N. Marchenkov, E.H. Conrad, P.N. First, W.A. de Heer Electronic confinement and coherence in patterned epitaxial graphene Science, 312 (2005), pp. 1191-1196

[7] K.V. Emtsev, A. Bostwick, K. Horn, J. Jobst, G.L. Kellogg, L. Ley, J.L. McChesney, T. Ohta, S.A. Reshanov, J. Röhrl, E. Rotenberg, A.K. Schmid, D. Waldmann, H.B. Weber, T. Seyller Towards wafer-size graphene layers by atmospheric pressure graphitization of silicon carbide Nat. Mater., 8 (2009), pp. 203-207

[8] K.S. Kim, Y. Zhao, H. Jang, S.Y. Lee, J.M. Kim, K.S. Kim, J.-H. Ahn, P. Kim, J.-Y. Choi, B.H. Hong Large-scale pattern growth of graphene films for stretchable transparent electrodes Nature, 457 (2009), pp. 706-710

[9] X. Li, W. Cai, J. An, S. Kim, J. Nah, D. Yang, R. Piner, A. Velamakanni, I. Jung, E. Tutuc, S.K. Banerjee, L. Colombo, R.S. Ruoff Large-area synthesis of high-quality and uniform graphene films on cooper foils Science, 324 (2009), pp. 1312-1314

[10] A. Dato, V. Radmilovic, Z. Lee, J. Phillips, M. Frenklach Substrate-free gas-phase synthesis of graphene sheets Nano Lett., 8 (2008), pp. 2012-2016

[11] O.C. Compton, S.T. Nguyen Graphene oxide, highly reduced graphene oxide, and graphene: versatile building blocks for carbon-based materials Small, 6 (2010), pp. 711-723

[12] B.C. Brodie On the atomic weight of graphite Philos. Trans. R. Soc. Lond., 149 (1859), pp. 249-259

[13] W.S. Hummers, R.E. Offeman Preparation of graphitic oxide J. Am. Chem. Soc., 80 (1958), p. 1339

[14] S. Park, R.S. Ruoff Chemical methods for the production of graphenes Nat. Nanotechnol., 4 (2009), pp. 217-224

[15] G. Eda, C. Mattevi, H. Yamaguchi, H. Kim, M. Chhowalla Insulator to semimetal transition in graphene oxide J. Phys. Chem. C, 113 (2009), pp. 15768-15771

[16] A. Lerf, H. He, M. Forster, J. Klinowski Structure of graphite oxide revisited J. Phys. Chem. B, 102 (1998), pp. 4477-4482

[17] K. Erickson, R. Erni, Z. Lee, N. Alem, W. Gannett, A. Zettl Determination of the local chemical structure of graphene oxide and reduced graphene oxide Adv. Mater., 22 (2010), pp. 4467-4472

[18] M. Acik, C. Mattevi, C. Gong, G. Lee, K. Cho, M. Chhowalla, Y.J. Chabal The role of intercalated water in multilayered graphene oxide ACS Nano, 4 (2010), pp. 5861-5868

[19] D.R. Dreyer, S. Park, C.W. Bielawski, R.S. Ruoff The chemistry of graphene oxide Chem. Soc. Rev., 39 (2010), pp. 228-240

[20] G. Eda, Y.-Y. Lin, C. Mattevi, H. Yamaguchi, H.-A. Chen, I.-S. Chen, C.-W. Chen, M. Chhowalla Blue photoluminescence from chemically derived graphene oxide Adv. Mater., 22 (2010), pp. 505-509

[21] J.-L. Chen, X.-P. Yan, K. Meng, S.-F. Wang Graphene oxide based photoinduced charge transfer label-free near-infrared fluorescent biosensor for dopamine Anal. Chem., 83 (2011), pp. 8787-8793

[22] K.P. Loh, Q. Bao, G. Eda, M. Chhowalla Graphene oxide as a chemically tunable platform for optical applications Nat. Chem., 2 (2010), pp. 1015-1024

[23] M. Li, S.K. Cushing, X. Zhou, S. Guo, N.Q. Wu Fingerprinting photoluminescence of functional groups in graphene oxide J. Mater. Chem., 22 (2012), pp. 23374-23379

[24] L. Han, P. Wang, S. Dong Progress in graphene-based photoactive nanocomposites as a promising class of photocatalyst Nanoscale, 4 (2012), pp. 5814-5825

[25] M. Jahan, Q. Bao, K.P. Loh Electrocatalytically active graphene-porphyrin MOF composite for oxygen reduction reaction J. Am. Chem. Soc., 134 (2012), pp. 6707-6713

[26] Q.Y. He, S.X. Wu, Z.Y. Yin, H. Zhang Graphene-based electronic sensors Chem. Sci., 3 (2012), pp. 1764-1772

[27] T.-H. Han, Y.-K. Huang, A.T.L. Tan, V.P. Dravid, J.-X. Huang Steam etched porous graphene oxide network for chemical sensing J. Am. Chem. Soc., 133 (2011), pp. 15264-15267

[28] N.D. Mermin Crystalline order in two dimensions Phys. Rev., 176 (1968), pp. 250-254

[29] Y. Si, E.T. Samulski Exfoliated graphene separated by platinum nanoparticles Chem. Mater., 20 (2008), pp. 6792-6797

[30] Z.G. Xiong, L.L. Zhang, J.Z. Ma, X.S. Zhao Photocatalytic degradation of dyes over graphene-gold nanocomposites under visible light irradiation Chem. Commun., 46 (2010), pp. 6099-6101

[31] K.-S. Kim, I.-J. Kim, S.-J. Park Influence of Ag doped graphene on electrochemical behaviors and specific capacitance of polypyrrole-based nanocomposites Synt. Met., 160 (2010), pp. 2355-2360

[32] K. Krishnamoorthy, M. Veerapandian, K. Yun, S.-J. Kim The chemical and structural analysis of graphene oxide with different degrees of oxidation Carbon, 53 (2013), pp. 38-49

[33] I.K. Moon, J. Lee, R.S. Ruoff, H. Lee Reduced graphene oxide by chemical graphitization Nat. Commun., 1 (2010), pp. 73-78

[34] L. Liu, J. Liu, Y. Wang, X. Yan, D.D. Sun Facile synthesis of monodispersed silver nanoparticles on graphene oxide sheets with enhanced antibacterial activity New J. Chem., 35 (2011), pp. 1418-1423

[35] X.-Z. Tang, Z. Cao, H.-B. Zhang, J. Liu, Z.-Z. Yu Growth silver nanocrystals on graphene by simultaneous reduction of graphene oxide and silver ions with a rapid and efficient one-step approach Chem. Commun., 47 (2011), pp. 3084-3086

[36] A.C. Ferrari, J. Robertson Raman of spectroscopy amorphous, nanostructured, diamond-like carbon, and nanodiamond Philos. Trans. R. Soc. Lond. A, 362 (2004), pp. 2477-2512

[37] A.C. Ferrari, J.C. Meyer, V. Scardaci, C. Casiraghi, M. Lazzeri, F. Mauri, S. Piscanec, D. Jiang, K.S. Novoselov, S. Roth, A.K. Geim Raman spectrum of graphene and graphene layers Phys. Rev. Lett., 97 (2006), pp. 187401-187404

[38] A.M. Dimiev, L.B. Alemany, J.M. Tour Graphene oxide. Origin of acidity, its instability in water, and a new dynamic structural model ACS Nano, 7 (2013), pp. 576-588

[39] J. Zhang, Z. Xiong, X.S. Zhao Graphene-metal-oxide composites for the degradation of dyes under visible light irradiation J. Mater. Chem., 21 (2011), pp. 3634-3640

[40] B. Konkena, S. Vasudevan Understanding aqueous dispersibility of graphene oxide and reduced graphene oxide through pKa measurement J. Phys. Lett., 3 (2012), pp. 867-872

[41] T. Shen, Z.-G. Zhao, Q. Yu, H.-J. Xu Photosensitized reduction of benzil by heteroatom-containing anthracene dyes J. Photochem. Photobiol. A, 47 (1989), pp. 203-212

[42] Z. Xiong, L.L. Zhang, J. Ma, X.S. Zhao Visible-light-induced dye degradation over copper-modified reduced graphene oxide Chem. Eur. J., 17 (2011), pp. 2428-2434

[43] S. Dunn, S. Sharp, S. Burgess The photochemical growth of silver nanoparticles on semiconductor surfaces-initial nucleation stage Nanotechnology, 20 (2009), pp. 115604-115609

[44] A. Mozumder, J.L. Magee Model of tracks of ionizing radiation for radical reaction mechanisms Radiat. Res., 28 (1966), pp. 203-214

[45] T. Ji, Y. Hua, M. Sun, N. Ma The mechanism of the reaction of graphite oxide to reduced graphene oxide under ultraviolet irradiation Carbon, 54 (2013), pp. 412-418

[46] I.V. Lightcap, S. Murphy, T. Schumer, P.V. Kamat Electron hopping through single-to-few-layer graphene oxide films. Side-selective photocatalytic deposition of metal nanoparticles J. Phys. Chem. Lett., 3 (2012), pp. 1453-1458

[47] H. Sun, S. Liu, G. Zhou, H.M. Ang, S. Wang, M.S. Tadé Reduced graphene oxide for catalytic oxidation of aqueous organic pollutants Appl. Mater. Interfaces, 4 (2012), pp. 5466-5471

[48] L.F. Velasco, V. Maurino, E. Laurenti, I.M. Fonseca, J.C. Lima, C.O. Ania Photoinduced reactions occurring on activated carbons. A combined photooxidation and ESR study Appl. Ctal. A: General, 352 (2013), pp. 1-8

[49] Z. Tang, Y. Lei, B. Guo, L. Zhang, D. Jia The use of rhodamine B-decorated graphene as a reinforcement in polyvinyl alcohol composites Polymer, 53 (2012), pp. 673-680

[50] X. Chen, G. Wu, J. Chen, X. Chen, Z. Xie, X. Wang Synthesis of clean and well-dispersive Pd nanoparticles with excellent electrocatalytic property on graphene oxide J. Am. Chem. Soc., 133 (2011), pp. 3693-3695

[51] H. Liao, D. Stenman, M. Jonsson Study of indigo carmine as radical probe in photocatalysis J. Photochem. Photobiol. A: Chem., 202 (2009), pp. 86-91

[52] A. Mittal, J. Mittal, L. Kurup Batch and bulk removal of hazardous dye, indigo carmine from wastewater through adsorption J. Hazard. Mater., 137 (2006), pp. 591-602

[53] G.K. Ramesha, A. Vijaya Kumara, H.B. Muralidhara, S. Sampath Graphene and graphene oxide as effective adsorbents toward anionic and cationic dyes J. Colloid. Interface Sci., 361 (2011), pp. 270-277

[54] P. Sharma, M.R. Das Removal of a cationic dye from aqueous solution using graphene oxide nanosheets: investigation of adsorption parameters J. Chem. Eng. Data, 58 (2013), pp. 151-158

[55] Y. Matsumoto, M. Koinuma, S. Ida, S. Hayami, T. Taniguchi, K. Hatakeyama, H. Tateishi, Y. Watanabe, S. Amano Photoreaction of graphene oxide nanosheets in water J. Phys. Chem. C, 115 (2011), pp. 19280-19286

[56] R. Gómez, T. López, E. Ortiz-Islas, J. Navarrete, E. Sánchez, F. Tzompantzi, X. Bokhimi Effect of sulfation on the photoactivity of TiO2 sol-gel derived catalysts J. Mol. Catal. A: Chem., 193 (2003), pp. 217-226
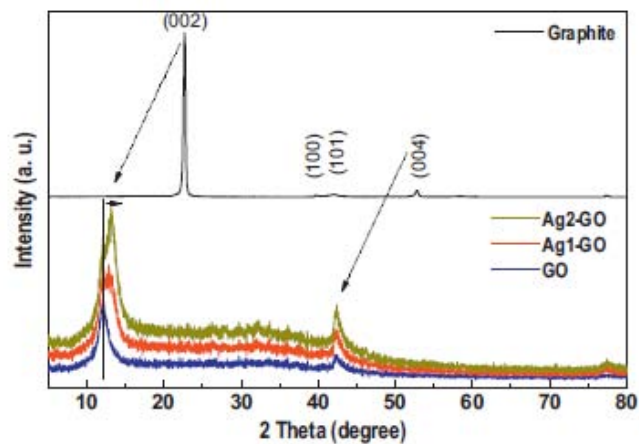
Fig. 1: XRD patterns of the precursor of graphite, graphene oxide and Ag1-GO and Ag2-GO nanocomposites. The main peaks of graphite pristine are also included in the figure for reference (JCPDS 41-1487).
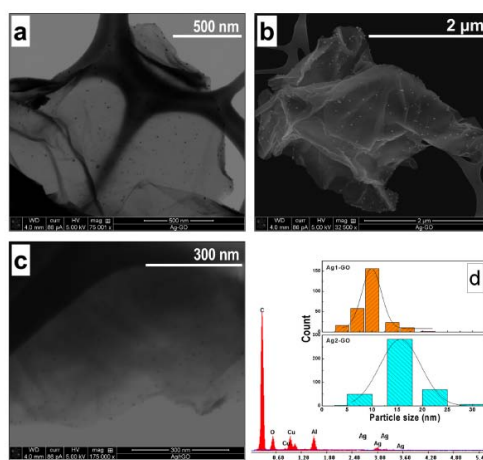

Fig. 2: FESEM images of the AgNPs decorated by the UV photoreduction method on GO: (a) FESEM image of the nanocomposite Ag1-GO, dark silver nanoparticles were detected over all the GO sheets, (b) FESEM image Ag2-GO bright catalyst silver nanoparticles were detected over the GO, (c) FESEM image Ag2-GO nanocomposite with a reduction process with DMF (Ag2-GOPR), showing analogous highly dispersion of AgNPs than samples without reduction (d) EDS and histograms obtained from AgNPs nanocomposites. In the case of Ag1-GO the mean size is 10 nm, and for Ag2-GO is 15 nm.
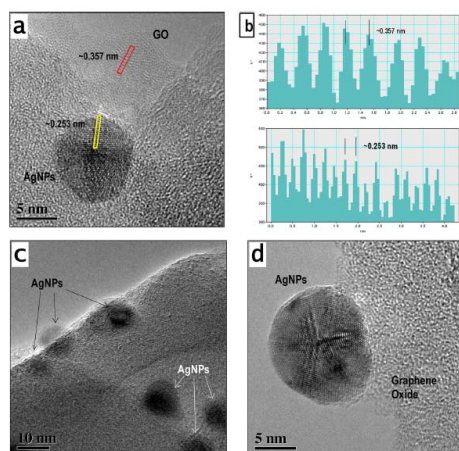
11

Fig. 3: Selected TEM images of the Ag1-GO nanocomposite, (a) HRTEM of a quasi-spherical AgNPs showing the fringes of plane (1 1 1), and the cross-section of a stack of GO in (b) profile of fringes for GO and AgNPs, (c) TEM image of several AgNPs dispersed on GO, and (d) HRTEM of quasi-spherical AgNP in the edge of a GO sheet.
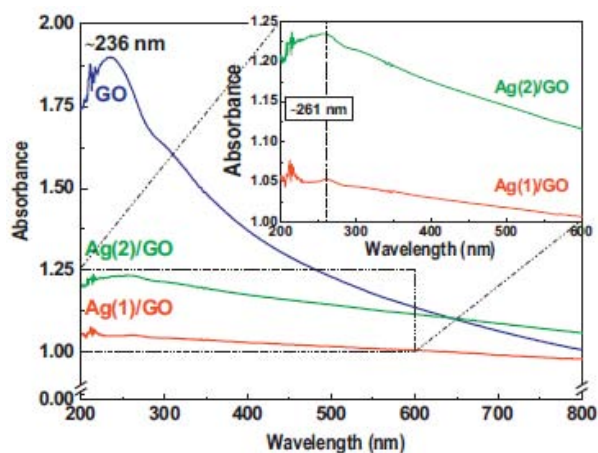

Fig. 4: UV-vis spectra of GO and AgNPs-GO nanocomposites. The inset indicates the corresponding UV-vis spectra in the range from 200 to 600 nm in order to compare the absorption band around 260 nm.
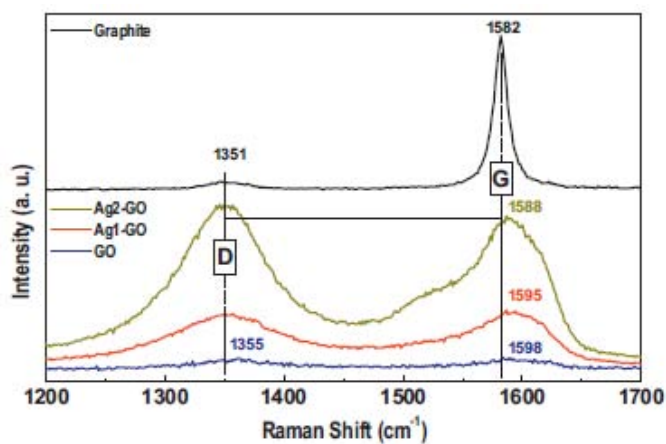

Fig. 5: Raman spectra of AgNPs-GO nanocomposites and GO compared with pristine graphite
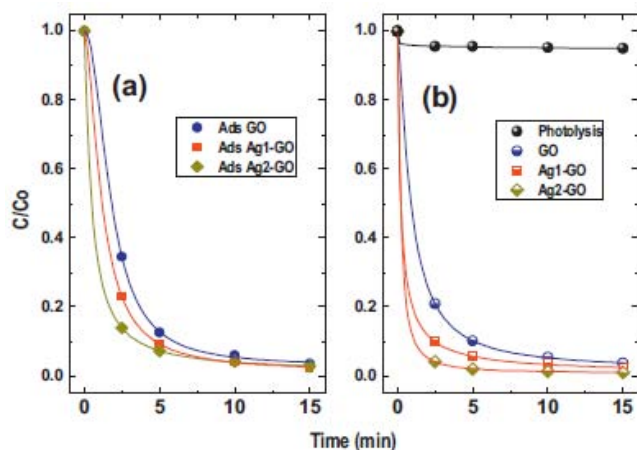
12

Fig. 6: (a) Adsorption in dark condition of Rhodamine B as a function of time over GO and AgNPs-GO nanocomposites. (b) Degradation of Rhodamine B as a function of time over GO and AgNPs-GO nanocomposites under visible-light irradiation.
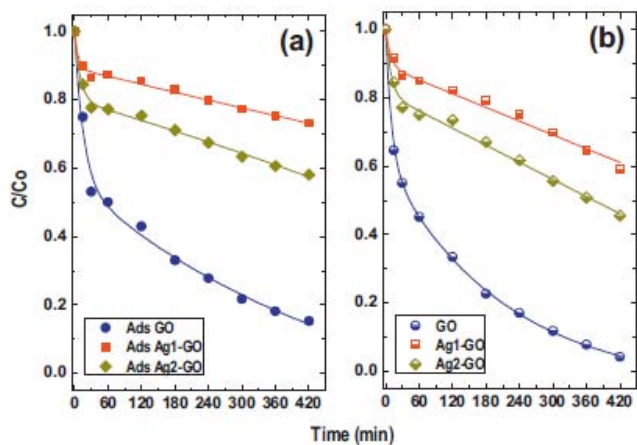

Fig. 7: (a) Adsorption in dark condition of Indigo Carmine as a function of time over GO and AgNPs-GO nanocomposites. (b) Degradation of Indigo Carmine as a function of time over GO and AgNPs-GO nanocomposites under visible-light irradiation.
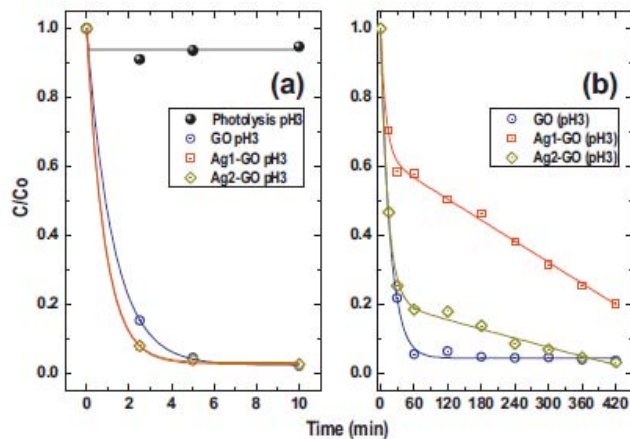

Fig. 8: (a) Degradation of RhB as a function of time over GO and AgNPs-GO nanocomposites under visible-light irradiation at pH 3. (b) Degradation of Indigo Carmine as a function of time over GO and AgNPs-GO nanocomposites under visible-light irradiation at pH 3.
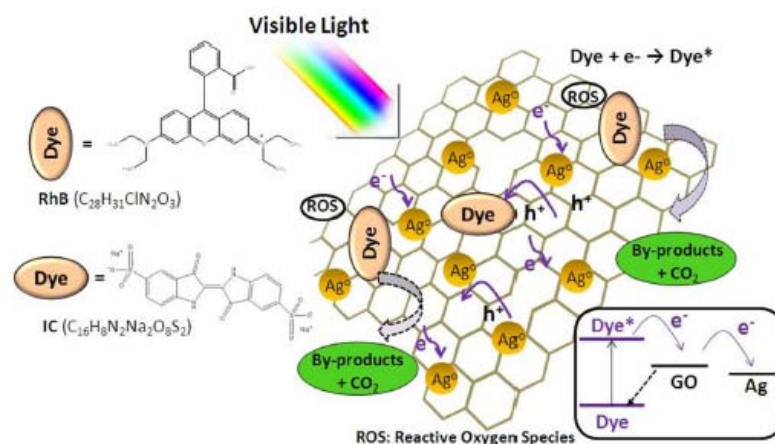
Fig. 9: Schematic representation of the possible way of decomposition of RhB and IC dyes over the graphene-silver nanocomposites, based on Ref. [30].

Table 1
Kinetic parameters of adsorption and visible light degradation of RhB and IC for GO and AgNPs/GO composites. The apparent rate constant was estimated by plotting $\ln(C_0/C)$ versus time.

Rhodamine (RhB)	Conversion (%)[a]	K (min^{-1})	$t_{1/2}$ (min)
Adsorption GO	95	0.31	2.2
Adsorption Ag1-GO	97	0.38	1.8
Adsorption Ag2-GO	98	0.40	1.7
Photocatalyst GO	96	0.34	2
Photocatalyst Ag1-GO	98	0.46	1.5
PhotocatalystAg2-GO	99	0.53	1.3

Indigo Carmine (IC)	Conversion (%)[a]	K (min^{-1})	$t_{1/2}$ (h)
Adsorption GO	86	0.004	2.8
Adsorption Ag1-GO	28	0.0005	23
Adsorption Ag2-GO	43	0.001	11.6
Photocatalyst GO	96	0.007	1.6
Photocatalyst Ag1-GO	40	0.001	11.6
PhotocatalystAg2-GO	54	0.0015	7.6

[a] % conversion for RhB at 10 min and for IC at 7 h.

Fig. 10:

Table 2
Kinetic parameters of adsorption and visible light degradation of RhB and IC for GO and AgNPs/GO composites and acid conditions, pH 3 with H_2SO_4. The apparent rate constant was estimated by plotting $\ln(C_0/C)$ versus time.

Rhodamine (RhB)	Conversion (%)[a]	K (min^{-1})	$t_{1/2}$ (min)
GO at pH 3	98	0.5	1.4
Ag1-GO at pH 3	99	0.7	1
Ag2-GO at pH 3	99	0.7	1

Indigo Carmine (IC)	Conversion (%)[a]	K (min^{-1})	$t_{1/2}$ (h)
GO at pH 3	97	0.045	0.25
Ag1-GO at pH 3	76	0.003	3.8
Ag2-GO at pH 3	97	0.0065	1.75

[a] % conversion for RhB at 5 min and for IC at 6 h.

Fig. 11:

14